Materials Science and Engineering B 291 (2023) 116314

Contents lists available at ScienceDirect

Materials Science & Engineering B

journal homepage: www.elsevier.com/locate/mseb

Cluster-layered $[Fe/Cr]_{30}$ structure exhibited Kondo-like effect studied by GISAXS and Mössbauer spectroscopy

R.A. Baulin [a,b,*], M.A. Andreeva [a], A.V. Rogachev [b], Yu.L. Repchenko [b], S.N. Yakunin [b], M.A. Milyaev [c], D.A. Ponomarev [c], L.N. Romashev [c], V.V. Ustinov [c]

[a] Lomonosov Moscow State University, Faculty of Physics, Moscow 119991, Russia
[b] National Research Centre "Kurchatov Institute", Moscow 123182, Russia
[c] M.N. Mikheev Institute of Metal Physics UB RAS, 620990 Ekaterinburg, Russia

ARTICLE INFO

Keywords:
Cluster-layered nanostructures
Mössbauer spectroscopy
Kondo-like effect
X-ray reflectometry

ABSTRACT

Structure and morphology of epitaxial $[Fe/Cr]_{30}$ multilayers with ultrathin Fe layers (nominally 0.12 nm and 0.08 nm) have been investigated by X-ray reflectivity, synchrotron Mössbauer spectroscopy at low temperature and grazing-incidence small angle X-ray scattering (GISAXS). The films demonstrate Kondo-like behavior of electrical resistivity. The GISAXS patterns reveal their cluster-layered structure. The observed side maxima give the information about the sizes and distances between lateral inhomogeneities. Mössbauer reflectivity spectra measured below the critical angle of the total reflection support the existence of the cluster-layered structure of the samples. Magnetic hyperfine field distributions show that largest number of ^{57}Fe atoms is situated in interfaces of iron clusters and their number increases in the thinnest films.

1. Introduction

Nanoscale metallic multilayers possess a wide range of outstanding properties: the giant magnetoresistance (GMR) [1,2], oscillating interlayer exchange coupling [3,4], ladder-like magnetization curve [5], multiple spin–flip transitions [6], perpendicular magnetic anisotropy [7–11], anomalous Hall effect [12–17], enhanced interfacial Dzyaloshinskii–Moriya interactions [18–19], formation of magnetic bubbles or skyrmions [20–21] and so on. All these effects are important for applications in spintronics, sensorics, quantum optics, etc [22–23]. A large variety of properties can be achieved by the variations of the elemental composition of the layers, their thicknesses, and quality of interfaces. For layer thicknesses in multilayer less than 0.3 nm their magnetic properties become even more intriguing. A decrease of the nominal thickness of the iron layers in Fe/Cr superlattices down to atomic dimensions at which these layers are not continuous is accompanied by appearance of the Kondo-like behavior of resistivity: with decreasing temperature the electrical resistivity not decreases but starts to increase from a certain temperature [24]. At room temperature such multilayers are superparamagnetic, at low temperatures the transition to spin glass (SG) state occurs [25]. Such behavior is not typical neither for Fe/Cr superlattices [26], nor for Fe-Cr-alloys [27]. The Kondo-like effect has been explained in [24] by a spin-dependent contribution to resistivity, originated from the electron scattering on the planes of magnetic clusters. Therefore, the details of created iron clusters, their lateral distributions and their effective magnetic moments are of peculiar interest.

Mössbauer spectroscopy presents an excellent test of the local environment of resonant nuclei. For example, Mössbauer method has evidenced of the inhomogeneous distribution of ^{57}Fe atoms in [Fe/Cr] sample with ultrathin Fe layers which is not possible to disclose by X-ray reflectivity method [28]. However, it does not give the peculiarities of the lateral structure of iron clusters, their size and shape.

Grazing incidence small-angular x-ray scattering (GISAXS) is the best technique for characterization nanoobjects on surfaces [29–33], buried nanoparticles [34], layers roughness [35–37], lateral inhomogeneity in multilayers [38–40]. It is even used to gain sub-picosecond time resolution for multilayers depth profiling in pump-probe experiments [41].

In this paper, we report the experimental proof of cluster-layered structure in [Fe/Cr] multilayers with ultrathin Fe layers, that had exhibited Kondo-like behavior, by means of low temperature Mössbauer spectroscopy and GISAXS measurements.

* Corresponding author at: Lomonosov Moscow State University, Faculty of Physics, Moscow 119991, Russia.
E-mail address: baulin.roman@physics.msu.ru (R.A. Baulin).

https://doi.org/10.1016/j.mseb.2023.116314
Received 8 September 2021; Received in revised form 20 October 2022; Accepted 22 January 2023
Available online 15 February 2023

2. Materials and methods

The [Fe(0.12 nm)/Cr(1.05 nm)]$_{30}$ and [Fe(0.08 nm)/Cr(1.05 nm)]$_{30}$ samples (the nominal thicknesses are given) were grown on Al_2O_3 substrate with 7 nm Cr buffer layer at the Katun'-C molecular-beam epitaxy facility in the Institute of Metal Physics (IMP) in Ekaterinburg, Russia. Iron layers were prepared with 95% enriched ^{57}Fe target in order to enhance Mössbauer signal. The samples were covered by 1.2 nm Cr layer to prevent oxidation.

The ultimate decrease of the ^{57}Fe nominal layer thickness in these multilayers leads to a very specific behavior of magnetoresistance for these samples (Fig. 1).

The increase of electrical resistance below 170 K for [Fe(0.12 nm)/Cr (1.05 nm)]$_{30}$ and below 242 K for [Fe(0.08 nm)/Cr(1.05 nm)]$_{30}$ sample takes place (Kondo-like effect [24]) and a strong dependence on the external magnetic field is observed. Previous experiments have shown that the minimum of the electrical resistance for [Fe(0.12 nm)/Cr(1.05 nm)]$_{30}$ sample correlates with beginning of the magnetic phase transition [28]. It is important to note that for the sample with smaller inhomogeneities the magnetic phase transition accompanied by the appearance of magnetoresistance appears at lower temperature of 100 K compared to 150 K for the sample with larger inhomogeneities, but the increase of the resistivity for smaller inhomogeneity sample started at higher temperature ~250 K comparing with 150 K for the sample with larger inhomogeneities.

Preliminary Mössbauer measurements were performed at room temperature (RT) with common radioactive ^{57}Co source. For both samples RT conversion electron Mössbauer spectra show just single line pattern confirming a superparamagnetic state of Fe atoms.

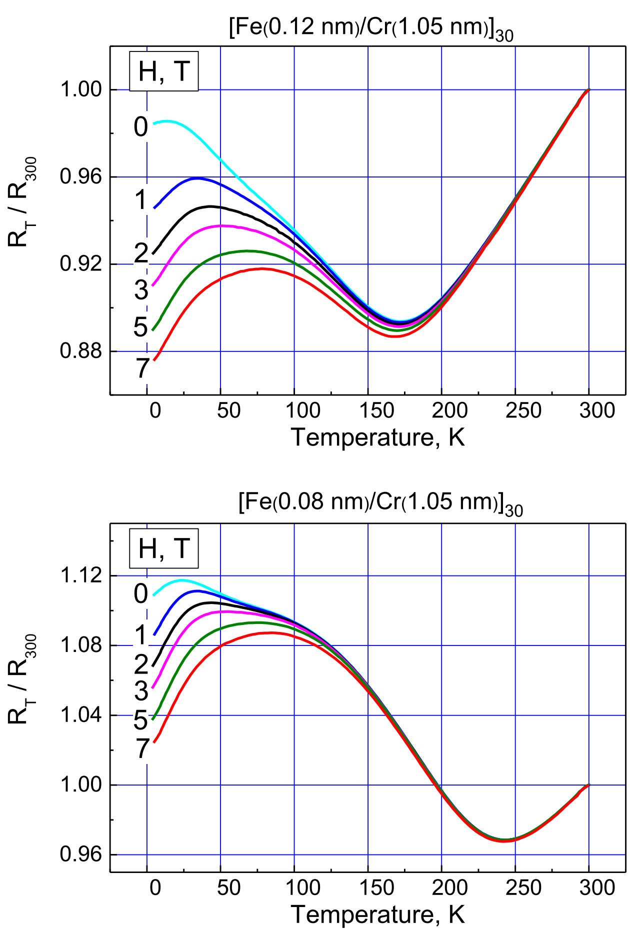

Fig. 1. Temperature dependence of the normalized electrical resistance R/R$_{300\ K}$ for the [Fe(0.12 nm)/Cr(1.05 nm)]$_{30}$ (top) and [Fe(0.08 nm)/Cr(1.05 nm)]$_{30}$ (bottom) multilayers at different magnetic field. Fig. 1 (top) is reproduced with the permission from [28].

Mössbauer investigations at low temperature were performed at the ID18 beamline [42] of the European Synchrotron Radiation Facility (ESRF) using the Synchrotron Mössbauer Source (SMS) [43]. The SMS is a nuclear resonant monochromator employing pure nuclear reflection (1 1 1) from an iron borate ($^{57}FeBO_3$) crystal. The source provides a pure π-polarized radiation at 14.4 keV photon energy within a bandwidth of 15 neV which is tunable in the energy range about ~0.6 μeV. The samples were placed into superconducting cryo-magnetic system and cooled down to 4 K. Mössbauer spectra were measured in reflection geometry (R-spectra) [44,45] at grazing incidence angle $\theta = 0.2^\circ$. The fit of the Mössbauer R-spectra was performed with REFSPC [46,47] software. X-ray reflectivity angular curves at 14.4 keV photon energy (0.086 nm wavelength) for which the super- monochromatization was not needed were measured with radiation from UmWeg reflection from $^{57}FeBO_3$ crystal supplying higher intensity than forbidden (1 1 1) reflection.

Grazing incidence small angular x-ray scattering (GISAXS) was measured at the "Langmuir" beamline of the Kurchatov specialized source of synchrotron radiation "KISI-Kurchatov". GISAXS patterns have been obtained at room temperature with monochromatic radiation (0.086 nm wavelength) at a fixed grazing incidence angle $\theta = 0.3^\circ$ which was 1.5 times larger than the critical angle ($\theta_c \sim 0.2^\circ$). Experiment geometry is presented at Fig. 2.

The size of incident beam was 50x50 μm. The scattering patterns were recorded by 2D LAMBDA 750 K detector (55x55 μm pixel size) placed on 620 mm from the sample. Between the sample and detector the vacuum flypass was mounted. The specular beam was suppressed by a beamstop and only diffuse scattering was recorded.

3. Results and discussion

The measured reflectivity curves (Fig. 3) show just one frequency Kiesig fringes determining the total multilayer thicknesses: that is H = 31.5 nm for [Fe(0.12 nm)/Cr(1.05 nm)]$_{30}$ sample including top and bottom interfaces and 31.0 nm for [Fe(0.08 nm)/Cr(1.05 nm)]$_{30}$ sample. The values are slightly smaller than the nominal values: 1.17 nm × 30 = 35.1 nm and 1.13 nm × 30 = 33.9 nm respectively. The root-mean-square surface roughness is evaluated as ~2.5 nm for both samples. The periodicity was not possible to detect, because the first order Bragg peak for 14.4 keV radiation could appear at ~2°. For such high angle and due to a very low contrast of electronic density for Cr and Fe cluster-layers mixed with Cr the reflected signal supposed to be too small. Moreover, a high difference between Fe and Cr layers' thicknesses

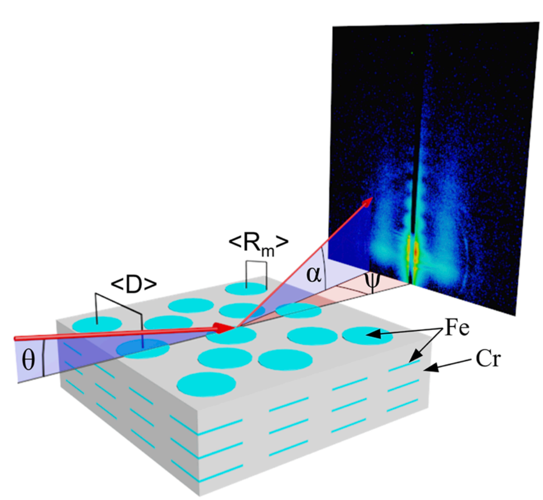

Fig. 2. Scattering geometry and sematic model of the sample.

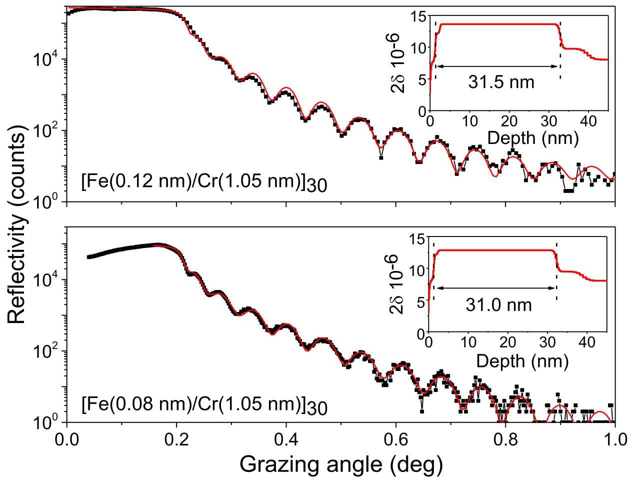

Fig. 3. X-ray reflectivity curves for [Fe(0.12 nm)/Cr(1.05 nm)]$_{30}$ (top) and [Fe (0.08 nm)/Cr(1.05 nm)]$_{30}$ (bottom) measured at $\lambda = 0.086$ nm (14.4 keV). Symbols are the experimental data; the lines are the fit result. In the inserts: depth profiles of the electronic density ($\propto 2\delta = -Re\chi^{el}$, χ^{el} is the real part of the electron susceptibility).

should strongly suppresses 1st Bragg reflection. Note that the previous measurements with 0.154 nm radiation for [Fe(0.12 nm)/Cr(1.05 nm)]$_{30}$ sample did not detect any Bragg peak (expected at ~3.7°) as well [28].

The precise fit of the X-ray reflectivity curve is an essential part of the GISAXS pattern interpretation because it allows to get the depth distribution of the total radiation field amplitudes at any angles for incident $E_i^{tot}(z,\theta)$ or scattered $E_f^{tot}(z,\alpha)$ radiation which are needed for calculation of the amplitudes of scattering waves by density inhomogeneities placed at any depth when we use the Distorted Wave Born Approximation (DWBA).

The measured GISAXS pattern (Fig. 4) as well has no any Bragg maximum evidence corresponding to the periodicity along depth (contrary to the sample with thicker (0.8 nm) Fe layers for which the Bragg maximum appeared in the GISAXS pattern [39]). Just Kiessig fringes along the angle of the scattered radiation above the surface plane α are presented. Basically the period of these oscillations can differ from that in the reflectivity curve because they correspond to the maximum depth at which the inhomogeneities are distributed. Clearly seen side peaks in the GISAXS pattern at $\psi = \pm 0.30°$ for [Fe(0.12 nm)/Cr(1.05 nm)]$_{30}$ and at $\psi = \pm 0.36°$ for [Fe(0.08 nm)/Cr(1.05 nm)]$_{30}$ characterize the correlations in the lateral distribution of inhomogeneities.

Simulation of the GISAXS pattern has been done by the Distorted Wave Born Approximation (DWBA). For calculation of the GISAXS in-

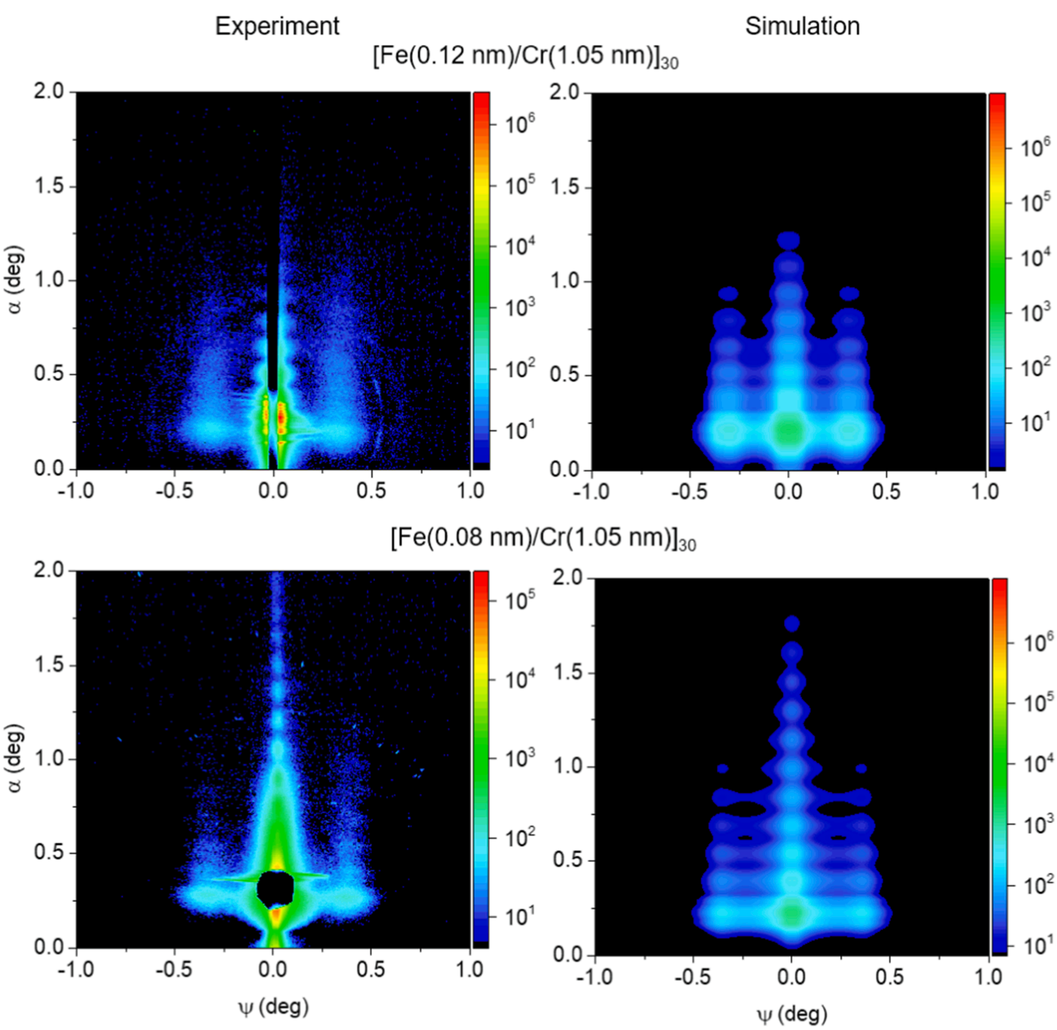

Fig. 4. Experimental (left) and simulated (right) GISAXS patterns for [Fe(0.12 nm)/Cr(1.05 nm)]$_{30}$ (top) and [Fe(0.08 nm)/Cr(1.05 nm)]$_{30}$ (bottom) samples at the grazing incidence angle $\theta = 0.3°$; α is the angle of the scattered radiation with the surface plane, ψ is the deviation angle from the specular reflection plane (See Fig. 2 for scattering geometry).

tensity $I(\vec{k}_i \rightarrow \vec{k}_f)$ the fine slicing of the structure (~0.1 nm) is used. In each of slice the amplitude of the total radiation field is beforehand calculated for the directions of the incident $E_i^{tot}(z, \theta)$ and outgoing $E_f^{tot}(z, \alpha)$ waves given by θ and α respectively with the help of propagation matrices. The modeling of inhomogeneities has been carried out as follows: in the slices relating to the iron layers and their interfaces with Cr layers they have the shape of disks of different radius (and the height equals to the thickness of the slice H_m) (see Fig. 2). In such a way a peculiar shape of the iron clusters can be taken into account.

The coherent sum of the scattering amplitudes by these inhomogeneities over all m slices determines the GISAXS intensity $I(\vec{k}_i \rightarrow \vec{k}_f)$ [39]:

$$I\left(\vec{k}_i \rightarrow \vec{k}_f\right) \propto \left| \sum_m E_i^{tot}(z_m, \theta) E_f^{tot}(z_m, \alpha) \bar{F}_{particle}\left(q^{\|}, z_m\right) \sqrt{W_m} \right|^2 S\left(q^{\|}\right) e^{-\sigma^{\perp 2} q^{\perp 2}} \tag{1}$$

where

$$q^{\perp} = \frac{2\pi}{\lambda}(\sin\theta + \sin\alpha), q^{\|} = \frac{2\pi}{\lambda}\sin\psi, \tag{2}$$

$\bar{F}_{particle}(q^{\|}, z_m)$ is a form factor of inhomogeneity (cluster), $S(q^{\|})$ is the interference function between waves scattered by lateral inhomogeneities in each slice. Factor $e^{-\sigma^{\perp 2} q^{\perp 2}}$ takes into account some loss of coherence in the interference of scattered waves from different slices with increasing angle, W_m is the relative "weight" of inhomogeneities in different slices,

Supposing an axial symmetry of inhomogeneities their form factor $\bar{F}_{particle}(q^{\|}, z_m)$ was taken in the form corresponding to the cylinder:

$$F_{particle}\left(q^{\|}, z_m\right) = 2\pi\, \Delta\rho_m\, H_m \sum_n \left(p_n R_n^2 \frac{J_1\left(q^{\|} R_n\right)}{q^{\|} R_n}\right) \Bigg/ \sum_n p_n \tag{3}$$

where additionally the averaging over its radius by Gauss function with width σ_m was applied:

$$p_n = e^{-\frac{(R_n - R_m)^2}{2\sigma_m}} \tag{4}$$

For the lateral correlation function $S(q^{\|})$ the simplest formula corresponding to the scattering by paracrystal was used [48–51]:

$$S\left(q^{\|}\right) = \frac{1 - P\left(q^{\|}\right)^2}{1 + P\left(q^{\|}\right)^2 - 2P\left(q^{\|}\right)\cos\left(q^{\|} D\right)} \tag{5}$$

with

$$P\left(q^{\|}\right) = \exp\left(-\frac{D}{\Lambda}\right) e^{\frac{-q^{\|2}\sigma_D^2}{2}} \tag{6}$$

where D is the nearest-neighbor distance between the inhomogeneities and σ_D is its root-mean-square deviation. In order to take into account a finite number of coherently scattering inhomogeneities, the $\exp(-\frac{D}{\Lambda})$ factor is inserted into (6) according to [50]. The parameter Λ is called the damping length. This factor allows us to take into account the scattering at $\psi = 0$ in the GISAXS pattern [29]. For [Fe(0.12 nm)/Cr(1.05 nm)]$_{30}$ GISAXS pattern calculation $\Lambda = 55$ nm and for [Fe(0.08 nm)/Cr(1.05 nm)]$_{30}$ $\Lambda = 44$ nm were used.

The fit of the horizontal (at $\alpha = 0.21°$) cross sections of the GISAXS pattern (see Fig. 5, left side) gives the average radius of iron clusters $R_m = 5.4$ nm with distribution $\sigma_m = 2$ nm and average distance between them $D = 15.4$ nm with distribution $\sigma_D = 2$ nm for [Fe(0.12 nm)/Cr(1.05 nm)]$_{30}$ sample; accordingly $R_m = 4$ nm, σ_m=1.6 nm, D=12.6 nm and $\sigma_D = 2.2$ nm for [Fe(0.08 nm)/Cr(1.05 nm)]$_{30}$ sample. It is remarkable that so small difference in cluster sizes R_m for two samples has so strong impact on the behavior of their electrical resistivity (Fig. 1).

The fit of the vertical cross sections (at $\psi = 0°$) of the GISAXS pattern (Fig. 5, right side) gives the maximal depth of existed inhomogeneities

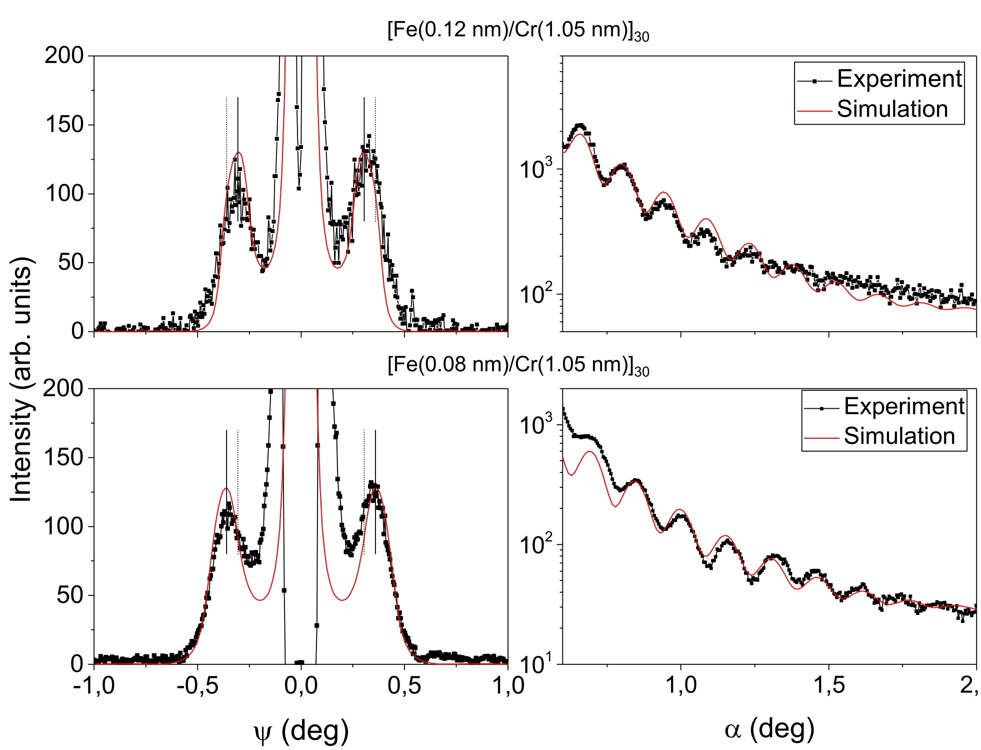

Fig. 5. Horizontal at $\alpha = 0.21°$ (left) and vertical at $\psi = 0°$ (right) cross sections of the GISAXS pattern for [Fe(0.12 nm)/Cr(1.05 nm)]$_{30}$ (top) and [Fe(0.08 nm)/Cr(1.05 nm)]$_{30}$ (bottom) samples. Symbols are the experimental data; the lines are the fit result. The difference in the maxima positions for two samples is designated by dash and solid vertical lines.

which is close to the total thickness of the multilayer determined from the oscillations on the X-ray reflectivity curve. We had to accept that the height of the iron clusters does not exceed several atomic layers, because if their vertical size H_z would be equal or larger the nominal period then the modulation of oscillations will takes place in the vertical scan, e.g. for $H_z = 1.5$ nm the first maximum of modulating oscillations will be observable at $\alpha \sim 3.3$, which is not the case. So we observed the formation of flattened iron clusters in $[Fe/Cr]_{30}$, the lateral size of which is much higher their height. In other words, we have got the experimental evidence of the existence of the planes of clusters which is the working model for the explanation of the Kondo-like behavior of these multilayers.

The measured Mössbauer R-spectra for the both samples at 4 K display a poorly resolved magnetic hyperfine splitting (Fig. 6). They were fitted with broad distributions of the magnetic hyperfine field B_{hf} which were thereafter approximated by 7 sextets with the same values of $B_{hf}^{(i)}$ (3.3 T, 6.9 T, 10.0 T, 12.5 T, 15.7 T, 19.5 T and 23.7 T) but their weights for the two samples were fitted. Each multiplet corresponds for the special number of Cr atoms as the nearest neighbors of ^{57}Fe atom. The smaller $B_{hf}^{(i)}$ correspond to the Fe atoms situated at the cluster interfaces. Therefore, the increase of relative weights of the smaller $B_{hf}^{(i)}$ for the sample with thinner iron layers (compare top and bottom distributions in Fig. 6) indicates that the size of the clusters in this sample is smaller.

The obtained from fit B_{hf} distributions are different from the binomial atom distribution in Fe_xCr_{1-x} alloy for $x \sim 0.12/(0.12 + 1.05) \approx 0.1$ and for $x \sim 0.08/(0.08 + 1.05) \approx 0.07$ (Fig. 7) but looks like typical for the Fe clusters with dominant interface regions. The average value of B_{hf} is evaluated as 11.6 T for the sample with thicker Fe layers and 9.7 T for the sample with thinner Fe layers. The fully absence of $B_{hf}^{(i)} = 33$ T at hyperfine distribution indicates that the vertical size of the clusters does not exceed the thickness of the iron layer including interfaces. That is in agreement with GISAXS results. The absence of the modulations of the thickness oscillations on the vertical GISAXS cross sections on the observable scale confirms the small vertical size of the clusters in out films.

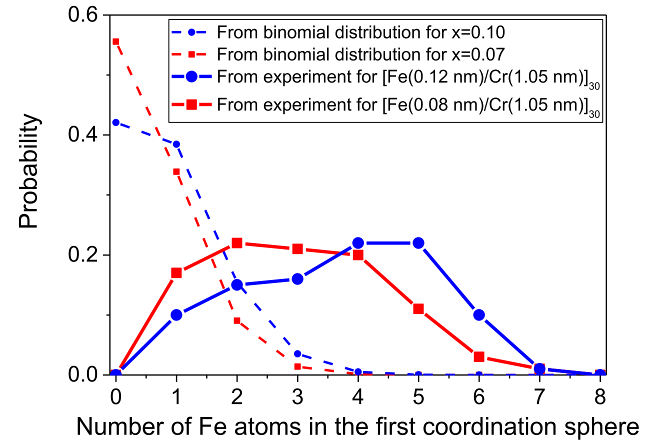

Fig. 7. Probability of the different Fe environments in Fe_xCr_{1-x} for different Fe concentrations × following from the binomial law (dash lines). The thick curves present the experimental results obtained from Mössbauer spectra.

4. Conclusion

We have performed X-ray and Mössbauer studies of $[Fe/Cr]_{30}$ multilayers with ultrathin iron layers demonstrated Kondo-like effect of electrical resistivity. We established the existence of the lateral inhomogeneity in films and iron cluster formation via GISAXS method. For the sample with nominal 0.12 nm Fe layer the average lateral size of the cluster and average distance between neighbor cluster $R_m = 5.4$ nm, D=15.4 nm was determined and for the sample with nominal 0.08 nm Fe layer we get $R_m = 4$ nm, D=12.6 nm. This means that such small difference in the parameters of the cluster-layered samples leads to the essential difference in the Kondo-like electrical resistance behavior and magnetoresistance with temperature. Decreasing R_m from 5.4 down to 4 nm shifts the minimum of the electrical resistance from 150 K to 250 K. The existence of the cluster-layered structure of the investigated samples is supported as well by Mössbauer measurements at 4 K. They give the magnetic hyperfine field distributions obtained from Mössbauer R-

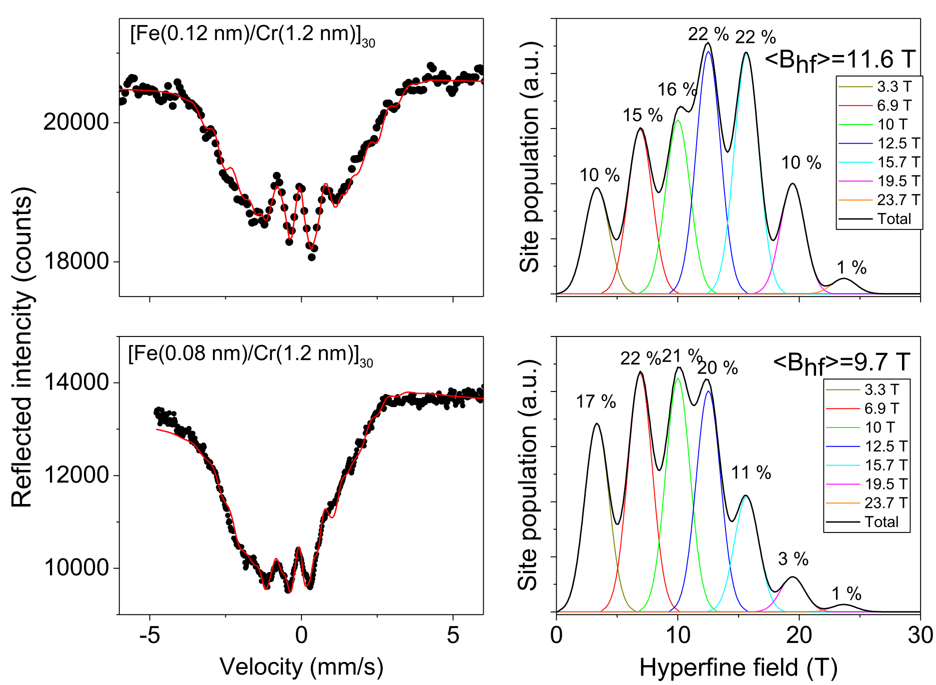

Fig. 6. Mössbauer R-spectra measured at 0.2° grazing angle (left) and magnetic hyperfine field distribution (right) for $[Fe(0.12\ nm)/Cr(1.05\ nm)]_{30}$ (top) and $[Fe(0.08\ nm)/Cr(1.05\ nm)]_{30}$ (bottom) samples.

spectra are essentially different from the case of homogeneous Fe_xCr_{1-x} ($x \cong 0.1$) alloys. Mössbauer R-spectra indicate as well that the thickness of the iron clusters does not exceed ~3–4 atomic layers and supports the idea explaining Kondo-like behavior by the electron spin-depending scattering on the planes of magnetic clusters [24]. The determined value of the average magnetic hyperfine field for the iron clusters (11.6 T for the sample with thicker Fe layers and 9.7 T for the sample with thinner Fe layers) can be helpful in determination of their effective magnetic moments, needed for further development of the theory Kondo-like effect.

Declaration of Competing Interest

The authors declare that they have no known competing financial interests or personal relationships that could have appeared to influence the work reported in this paper.

Data availability

Data will be made available on request.

Acknowledgements

The authors are grateful to A.I. Chumakov, R. Rüffer, D. Bessas (ESRF) for helping with synchrotron Mössbauer experiment. The reseatch at Lomonosov Moscow State University was supported by Ministry of Science and Higher Education of the Russian Federation (grant 075-15-2021-1353). The research at IMP RAS (Ekaterinburg) was carried out within the state assignment of the Russian Ministry of Education and Science (theme "Spin" No. AAAA-A18-118020290104-2). The authors acknowledge the NRC "Kurchatov Institute" for provision of synchrotron radiation resources at "Langmuir" beamline (project 1202) and European Synchrotron Radiation Facility for provision of synchrotron radiation resources at the beamline ID18 (projects MA-3217 and MA-4429).

References

[1] M.N. Baibich, J.M. Broto, A. Fert, F.N. Van Dau, F. Petroff, P. Eitenne, G. Creuzet, A. Friederich, J. Chazelas, Giant magnetoresistance of (001)Fe/(001)Cr magnetic superlattices, Phys. Rev. Lett. 61 (1988) 2472–2475.
[2] G. Binasch, P. Grünberg, F. Saurenbach, W. Zinn, Enhanced magnetoresistance in layered magnetic structures with antiferromagnetic interlayer exchange, Phys. Rev. B 39 (1989) 4828–4830.
[3] S.S.P. Parkin, N. More, K.P. Roche, Oscillations in exchange coupling and magnetoresistance in metallic superlattice structures: Co/Ru, Co/Cr, and Fe/Cr, Phys. Rev. Lett. 64 (1990) 2304.
[4] L. Tsetseris, Byungchan Lee, and Yia-Chung Chang Phys, Interlayer exchange coupling in Fe/Cr multilayers, Rev. B 55 (1997) 11586.
[5] C. L'abbé, J. Meersschaut, W. Sturhahn, S.J. Jiang, T.S. Toellner, E.E. Alp, S. d. Bader, Nuclear Resonant Magnetometry and its Application to Fe/Cr Multilayers, Phys. Rev. Lett. 93 (2004), 037201.
[6] V.V. Ustinov, M.A. Milayev, L.N. Romashev, T.P. Krinitsina, A.M. Burkhanov, V. V. Lauter-Pasyuk, H.J. Lauter, Multiple spin–flip transitions and stairs-like GMR in Fe/Cr superlattices with uniaxial in-plane anisotropy, JMMM 300 (2006) e281.
[7] U. Gradmann, J. Miiller, Flat Ferromagnetic, Epitaxial 48Ni/52Fe(111) Films of few Atomic Layers, Phys. Status Solidi 27 (1968) 313.
[8] U. Gradmann, Ferromagnetism near surfaces and in thin films, Appl. Phys. 3 (1974) 161.
[9] P.F. Carcia, A.D. Meinholdt, A. Suna, Perpendicular magnetic anisotropy in Pd/Co thin film layered structures, Appl. Phys. Lett. 47 (1985) 178.
[10] F.J.A. den Broeder, W. Hoving, P.J.H. Bloemen, Magnetic anisotropy of multilayers, J. Magn. Magn. Mater. 93 (1991) 562.
[11] D. Weller, J. Stöhr, R. Nakajima, A. Carl, M.G. Samant, C. Chappert, R. Mégy, P. Beauvillain, P. Veillet, G.A. Held, Microscopic Origin of Magnetic Anisotropy in Au/Co/Au Probed with X-Ray Magnetic Circular Dichroism, Phys. Rev. Lett. 75 (1995) 3752.
[12] W. Vavra, C.H. Lee, F.J. Lamelas, H. He, R. Clarke, C. Uher, Magnetoresistance and Hall effect in epitaxial Co-Au superlattices, Phys. Rev. B. 42 (1990) 4889.
[13] S. Kim, S.R. Lee, J.D. Chung, Magnetic properties of Pd/Co multilayer films studied by Hall effect, J. Appl. Phys. 73 (1993) 6344.
[14] F. Tsui, B. Chen, D. Barlett, R. Clarke, C. Uher, Scaling behavior of giant magnetotransport effects in Co/Cu superlattices, Phys. Rev. Lett. 72 (1994) 740.
[15] C. Canedy, X. Li, G. Xiao, Large magnetic moment enhancement and extraordinary Hall effect in Co/Pt superlattices, Phys. Rev. B 62 (2000) 508.
[16] V. Keskin, B. Aktas, J. Schmalhorst, G. Reiss, H. Zhang, J. Weischenberg, Y. Mokrousov, Temperature and Co thickness dependent sign change of the anomalous Hall effect in Co/Pd multilayers: An experimental and theoretical study, Appl. Phys. Lett. 102 (2013), 022416.
[17] P. Zhang, K. Xie, W. Lin, W.u. Di, H. Sang, Anomalous Hall effect in Co/Ni multilayers with perpendicular magnetic anisotropy, Appl. Phys. Lett. 104 (2014), 082404.
[18] A. Samardak, A. Kolesnikov, M. Stebliy, L. Chebotkevich, A. Sadovnikov, S. Nikitov, A. Talapatra, J. Mohanty, A. Ognev, Enhanced interfacial Dzyaloshinskii-Moriya interaction and isolated skyrmions in the inversion-symmetry-broken Ru/Co/W/Ru films, Appl. Phys. Lett. 112 (2018), 192406.
[19] A. Cao, R. Chen, X. Wang, X. Zhang, S. Lu, S. Yan, B. Koopmans, W. Zhao, Enhanced interfacial Dzyaloshinskii—Moriya interactions in annealed Pt/Co/MgO structures, Nanotechnology 31 (2020), 155705.
[20] C. Moreau-Luchaire, C. Moutafis, N. Reyren, J. Sampaio, C.A.F. Vaz, N. Van Horne, K. Bouzehouane, K. Garcia, C. Deranlot, P. Warnicke, P. Wohlhüter, J.-M. George, M. Weigand, J. Raabe, V. Cros, A. Fert, Additive interfacial chiral interaction in multilayers for stabilization of small individual skyrmions at room temperature, Nat. Nanotechnol. 11 (2016) 444.
[21] S. Woo, K. Litzius, B. Krüger, M.-Y. Im, L. Caretta, K. Richter, M. Mann, A. Krone, R. M. Reeve, M. Weigand, P. Agrawal, I. Lemesh, M.-A. Mawass, P. Fischer, M. Kläui, G.S.D. Beach, Observation of room-temperature magnetic skyrmions and their current-driven dynamics in ultrathin metallic ferromagnets, Nat. Mater. 15 (2016) 501.
[22] A. Sáenz-Trevizo, A.M. Hodge, Nanomaterials by design: a review of nanoscale metallic multilayers, Nanotechnology 31 (2020), 292002.
[23] V. Baltz, A. Manchon, M. Tsoi, T. Moriyama, T. Ono, Y. Tserkovnyak, Antiferromagnetic spintronics, Rev. Mod. Phys. 90 (1) (2018), 015005.
[24] V.V. Ustinov, L.N. Romashev, M.A. Milayev, A.V. Korolev, T.P. Krinitsina, A. M. Burkhanov, Kondo-like effect in the resistivity of superparamagnetic clusterlayered Fe/Cr nanostructures, JMMM 300 (2006) 148.
[25] A.B. Drovosekov, N.M. Kreines, D.I. Kholin, A.V. Korolev, M.A. Milyaev, L. N. Romashev, V.V. Ustinov, Spin-glass state of Fe/Cr multilayer structures with ultrathin iron layers, JETP Lett. 88 (2008) 118.
[26] A.K. Majumdar, A.F. Hebard, Avinash Singh, D. Temple, Spin-dependent electrical transport in ion-beam sputter deposited Fe-Cr multilayers, Phys. Rev. B 65 (2002), 054408.
[27] J. Arajs, Electrical Resistivity of Dilute Chromium-Rich Chromium-Iron Alloys below 30 K, Phys. Stat. Sol. 37 (1970) 329.
[28] M.A. Andreeva, R.A. Baulin, A.I. Chumakov, R. Rüffer, G.V. Smirnov, Y. A. Babanov, D.I. Devyaterikov, B.Y. Goloborodsky, D.A. Ponomarev, L. N. Romashev, V.v. Ustinov, Field-temperature evolution of the magnetic state of [Fe(1.2 Å)/Cr(10.5 Å)]*30 sample by Mössbauer reflectometry with synchrotron radiation, JMMM 440 (2017) 225.
[29] G. Renaud, R. Lazzari, F. Leroy, Probing surface and interface morphology with Grazing Incidence Small Angle X-Ray Scattering, Surf. Sci. Rep. 64 (2009) 255.
[30] J.R. Levine, J.B. Cohen, Y.W. Chung, Thin film island growth kinetics: a grazing incidence small angle X-ray scattering study of gold on glass, Surf. Sci. 248 (1991) 215.
[31] D. Babonneau, I.R. Videnović, M.G. Garnier, P. Oelhafen, Morphology and size distribution of gold nanoclusters in a−C: H films studied by grazing incidence small-angle x-ray scattering, Phys. Rev. B 63 (2001), 195401.
[32] P. Müller-Buschbaum, Grazing incidence small-angle X-ray scattering: an advanced scattering technique for the investigation of nanostructured polymer films, Anal. Bioanal. Chem. 376 (2003) 3.
[33] M. Schwartzkopf, A. Buffet, V. Korstgens, E. Metwalli, K. Schlage, G. Benecke, J. Perlich, M. Rawolle, A. Rothkirch, B. Heidmann, G. Herzog, P. Muller-Buschbaum, R. Rohlsberger, R. Gehrke, N. Stribeck, S.V. Roth, From atoms to layers: in situ gold cluster growth kinetics during sputter deposition, Nanoscale 5 (2013) 5053.
[34] Z.h. Jiang, D.R. Lee, S. Narayanan, J. Wang, S.K. Sinha, Waveguide-enhanced grazing-incidence small-angle x-ray scattering of buried nanostructures in thin films, Phys. Rev. B 84 (2011), 075440.
[35] Gagan Sharma, Ajay Gupta, Mukul Gupta, Kai Schlage, H.-C. Wille, In situ small-angle x-ray and nuclear resonant scattering study of the evolution of structural and magnetic properties of an Fe thin film on MgO (001), Phys. Rev. B 92 (2015) 224403.
[36] H. Jiang, W. Hua, N. Tian, A. Li, X. Li, Y. He, Z. Zhang, In situ GISAXS study on the temperature-dependent performance of multilayer monochromators from the liquid nitrogen cooling temperature to 600 °C, Appl. Surf. Sci. 508 (2020), 144838.
[37] R.V. Medvedev, K.V. Nikolaev, A.A. Zameshin, D. IJpes, I.A. Makhotkin, S. N. Yakunin, A.E. Yakshin, F. Bijkerk, Low-energy ion polishing of Si in W/Si soft X-ray multilayer structures, J. Appl. Phys. 126 (2019), 045302.
[38] M. Jerčinović, N. Radić, M. Buljan, J. Grenzer, I. Delač-Marion, M. Kralj, I. Bogdanović-Radović, R. Hübner, P. Dubček, K. Salamon, S. Bernstorff, Self-assembled growth of Ni nanoparticles in amorphous alumina matrix, J. Nanopart. Res. 16 (2014) 2296.
[39] A.V. Ragulskaya, M.A. Andreeva, A.V. Rogachev, S.N. Yakunin, The investigation of [Fe/Cr] multilayer by GISAXS, Superlattices Microstruct. 125 (2019) 16.
[40] K.V. Nikolaev, S.N. Yakunin, I.A. Makhotkin, J. Rie, R.V. Medvedev, A. V. Rogachev, I.N. Trunckin, A.L. Vasiliev, C.P. Hendrikx, M. Gateshki, R.W. E. Kruijs, F. Bijkerk, Grazing-incidence small-angle X-ray scattering study of correlated lateral density fluctuations in W/Si multilayers, Acta Crystallographica. Sect. A: Foundations Adv. 75 (2) (2019) 342.

[41] L. Randolph, M. Banjafar, Th. R. Preston, T. Yabuuchi, M. Makita, N.P. Dover, Ch. Rödel, S. Göde, Y. Inubushi, G. Jakob, J. Kaa, A. Kon, J.K. Koga, D. Ksenzov, T. Matsuoka, M. Nishiuchi, M. Paulus, F. Schon, K. Sueda, Y. Sentoku, T. Togashi, M. Bussmann, T.E. Cowan, M. Kläui, C. Fortmann-Grote, L. Huang, A.P. Mancuso, Th. Kluge, Ch. Gutt, M. Nakatsutsumi, Nanoscale subsurface dynamics of solids upon high-intensity femtosecond laser irradiation observed by grazing-incidence x-ray scattering, Phys. Rev. Research 4 (2022), 03303.

[42] R. Rüffer, A.I. Chumakov, Nuclear Resonance Beamline at ESRF, Hyperfine Interact. 97/98 (1996) 589.

[43] V. Potapkin, A.I. Chumakov, G.V. Smirnov, J.-P. Celse, R. Rüffer, C. McCammon, L. Dubrovinsky, The ^{57}Fe synchrotron Mössbauer source at the ESRF, J. Synchrotron Rad. 19 (2012) 559.

[44] S. Bernstein, E.C. Campbell, Nuclear anomalous dispersion in ^{57}Fe by the method of total reflection, Phys. Rev. 132 (1963) 1625.

[45] M.A. Andreeva, R.A. Baulin, A.I. Chumakov, R. Rüffer, G.V. Smirnov, Y. A. Babanov, D.I. Devyaterikov, M.A. Milyaev, D.A. Ponomarev, L.N. Romashev, V. V. Ustinov, Nuclear resonance reflectivity from $[^{57}Fe/Cr]_{30}$ multilayer with Synchrotron Mössbauer Source, J. Synchrotron Radiat. 25 (2018) 473.

[46] M.A. Andreeva, Nuclear resonant reflectivity data evaluation with the «REFTIM» program, Hyperfine Interact. 185 (2008) 17.

[47] https://www.esrf.fr/Instrumentation/software/data-analysis/OurSoftware/REFTIM-1.

[48] R. Lazzari, IsGISAXS: a program for grazing-incidence small-angle X-ray scattering analysis of supported islands'', J. Applied Crystallography 35 (2002) 406.

[49] G. Vignaud, A. Gibaud, J. Wang, S.K. Sinha, J. Daillant, G. Grübeland, Y. Gallot, An X-ray scattering study of laterally modulated structures: the example of diblock copolymers, J. Phys.: Condens. Matter. 9 (1997) L125.

[50] B. K. Vainshtein, Diffraction of X-Rays by Chain Molecules (Elsevier, Amsterdam, 1966), Chap. V.

[51] F. Leroy, R. Lazzari, G. Renaud, Effects of near-neighbor correlations on the diffuse scattering from a one-dimensional paracrystal, Acta Cryst. A60 (2004) 565.